Available online at www.sciencedirect.com

SciVerse ScienceDirect

Ceramics International 39 (2013) 3823–3829

CERAMICS INTERNATIONAL

www.elsevier.com/locate/ceramint

Synthesis of TiO_2 nanoparticles on mesoporous aluminosilicate Al-SBA-15 in supercritical CO_2 for photocatalytic decolorization of methylene blue

Fei Chang[a,*], Gang Wang[a], Yunchao Xie[a], Min Zhang[a], Jian Zhang[a], Hai-Jian Yang[b,**], Xuefeng Hu[c,***]

[a]*School of Environment and Architecture, University of Shanghai for Science and Technology, Shanghai 200093, PR China*

[b]*Key Laboratory of Catalysis and Materials Science of the State Ethnic Affairs Commission & Ministry of Education, Hubei Province, Key Laboratory of Analytical Chemistry of the State Ethnic Affairs Commission, College of Chemistry and Materials Science, South-Central University for Nationalities, Wuhan 430074, PR China*

[c]*Key Laboratory of Coastal Zone Environmental Processes, Yantai Institute of Coastal Zone Research, Chinese Academy of Sciences, Yantai 264003, PR China*

Received 13 September 2012; received in revised form 18 October 2012; accepted 18 October 2012
Available online 26 October 2012

Abstract

In the present study, titania nanoparticles were first constructed on mesoporous aluminosilicate Al-SBA-15 in supercritical carbon dioxide (Sc-CO_2) and the resultant samples were characterized by a combination of various techniques, such as X-ray diffraction (XRD), nitrogen physisorption, ^{27}Al MAS NMR, UV–vis diffuse reflectance spectroscopy, and transmission electron microscopy (TEM). It was identified that the Al species incorporated samples retained structures similar to that of the parent SBA-15. In addition, the content of titania loading varied with reaction temperature and time in Sc-CO_2. As-synthesized TiO_2/Al-SBA-15 samples were evaluated in terms of photocatalytic decolorization of methylene blue in aqueous solutions. It was observed that all TiO_2/Al-SBA-15 samples showed satisfactory decolorization efficiency that was much higher than those of TiO_2/SBA-15 and commercial TiO_2 under identical conditions, which could be mainly attributed to the effective adsorption capability, resulting from the extension of specific surface area after substitution of Si species with Al species.

Keywords: D. TiO_2; Aluminosilicate; SBA-15; Supercritical carbon dioxide

1. Introduction

Heterogeneous photocatalysis through semiconductor nano-oxides is shown to be an attractive technology for the control of environmental pollution and has become one of the most active research fields in recent years [1,2]. Among various metal oxide semiconductors used, titania has been the most investigated one, due to the effective photocatalysis, long-term thermal and chemical stability, low cost, and non-toxicity [3–5]. However, the nanosized titania produced in general procedures is greatly limited for practical applications because of the low specific surface area without pore system in structure. Besides conglomeration, nanosized catalyst in aqueous is prone to create a milky suspension and thus difficult to recover after reaction [1].

To solve these problems, extensive efforts have been devoted to fabricate supports with favorable features, which may meet shortfalls, although sometimes supported titania possesses low elimination efficiency [6]. SBA-15, a new type of ordered hexagonal-array mesoporous silica with two-dimensional *p6mm* hexagonal structure, one-dimensional channels, thick walls, and high hydrothermal

*Corresponding author. Tel.: +86 21 55271722.
**Corresponding author. Tel.: +86 27 67842752.
***Corresponding author. Tel.: +86 535 2109157.
E-mail addresses: feichang@usst.edu.cn (F. Chang), yanghaijian@vip.sina.com (H.-J. Yang), xfhu@yic.ac.cn (X. Hu).

0272-8842/$ - see front matter © 2012 Elsevier Ltd and Techna Group S.r.l. All rights reserved.
http://dx.doi.org/10.1016/j.ceramint.2012.10.223

stability [7,8], has received much attention as a catalyst support [9–11]. In order to widen the application scope, numerous attempts have been made to incorporate heteroatoms into SBA-15 frame work, especially partial replacement of Si^{4+} ions by Al^{3+} ions, to enhance the hydrothermal stability and create new acid cites *via* direct-synthesis or post-synthesis grafting techniques [12–14]. Actually, direct-synthesis method is more favorable because it will not only enhance the hydrothermal stability and create new acid cites, but also extend the specific surface area to a certain extent [14]. These traits enable Al-SBA-15 as a suitable catalyst and support [13–17].

Sc-CO_2 with unique properties such as low viscosity, high diffusivity, near zero surface tension, ease of complete separation from the reaction products by simply controlling the temperature or pressure, *etc*, has been the focus of many researches for developing green processes to prepare nanostructured materials [18,19]. Good solvation properties of Sc-CO_2 are able to facilitate the transfer of metal precursors into SBA-15 channels to generate nanoparticles without blockage of mesopores. In addition, the solvents and impurities are easily removed after reaction, ensuring formation of pure materials [20]. Liu et al. [21] have prepared Ti-SBA-15 materials with Ti incorporated into the framework of SBA-15 in supercritical CO_2–ethanol solution through a post-synthesis. Han et al. [22] have produced monolayer and doublelayer of titanium dioxide grafted SBA-15 using a surface sol–gel process in Sc-CO_2. The obtained materials with large surface specific surface area, ordered channels, and confined titania nanoparticles, are beneficial to facilitate the photocatalytic processes. However, the preparation of titania nanoparticles over mesoporous Al-SBA-15 using Sc-CO_2 technique has not been reported yet, as far as we know.

In this investigation, fabrication of titania nanoparticles on mesoporous aluminosilicate Al-SBA-15 was first investigated by transfer and deposition of the titanium precursor with the assistance of Sc-CO_2. The resultant TiO_2/Al-SBA-15 samples were characterized with a collection of techniques. Similar Al-SBA-15 structure after loading titania was retained. These as-synthesized samples were used to decolorize methylene blue, a cationic thiazine dye, in aqueous solution. Interestingly, higher photodegradable efficiency could be found for TiO_2/Al-SBA-15 than that for TiO_2/SBA-15 and commercial TiO_2 under the same condition, as a result of the effective adsorption capability, resulting from the extension of specific surface area after substitution of Si species with Al species.

2. Materials and methods

2.1. Reagents

Ammonium chloride (NH_4Cl) and poly(ethylene glycol)-block-poly(propylene glycol)-block-poly(ethylene glycol) (pluronic P123, $EO_{20}PO_{70}EO_{20}$, $M_n \approx 5800$) were purchased from Sigma-Aldrich Chemicals. Commercial TiO_2 was bought from Acros Organics. Other reagents such as aluminum tri-*sec*-butoxide (Al(O-*sec*-Bu)$_3$,) tetrabutyl orthotitanate (TBOT), tetraethyl orthosilicate (TEOS), hydrochloric acid (HCl), and methylene blue (MB) were obtained from Sinopharm Chemical Reagent Co. Ltd. (Shanghai, China). All reagents were used without purification and all aqueous solutions were prepared with deionized water.

2.2. Preparation of aluminosilicate Al-SBA-15

The mesoporous aluminosilicate Al-SBA-15 was prepared according to the reference with a small modification [23]: TEOS (9 mL) and Al(O-*sec*-Bu)$_3$ (molar ratio of Si/Al = 20, 0.5 g) in an HCl aqueous solution (pH = 1.5, 10 mL) was stirred at 313 K over 3 h before adding to another HCl aqueous solution (pH = 1.5, 150 mL) containing P123 (4 g). The resultant mixture was further stirred at 313 K for 24 h, and then transferred into a Teflon-lined stainless steel autoclave and aged at 373 K for 48 h. After cooling down to room temperature, the product was filtered, repeatedly washed with NH_4Cl aqueous solution and distilled water, and dried overnight at 373 K in air. The target sample was finally obtained by calcination in air at heating rate of 2 K/min upto 823 K and maintaining at this temperature for 4 h to remove the copolymer template. As a reference, SBA-15 was also synthesized through a same procedure in the absence of aluminum source.

2.3. Preparation of TiO_2/Al-SBA-15 in Sc-CO_2

In the experimental, TBOT (0.2 mL) and Al-SBA-15 (0.4 g) were loaded on the bottom of the high-pressure stainless steel vessel (400 mL) and the small cage hanged underneath the lid, respectively. The small cage was covered with 100-mesh screen to ensure the transport and permeability of only molecular TBOT. The schematic diagram of experimental setup is shown in Fig. 1. After heating to a certain temperature, liquid CO_2 was pressed into the vessel by a syringe pump upto 20 MPa. The vessel was maintained at these conditions for an assigned time. Subsequently, the resultant solid was centrifuged, filtered, washed three times with ethanol, and dried at 373 K for

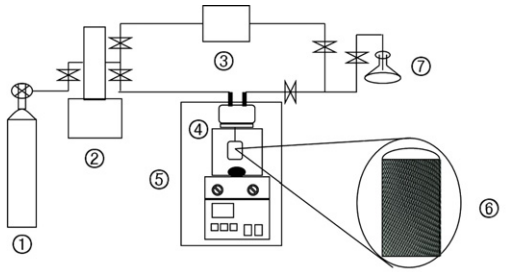

① CO_2 tank ② Syringe pump ③ Storing vessel ④ Reaction vessel ⑤ Magnetic stirrer and thermo control box ⑥ Small cage covered with screen ⑦ Waste bottle

Fig. 1. Schematic diagram of the apparatus.

24 h. The solid was calcined at 823 K for 5 h. By varying the reaction time and temperature, TiO_2/Al-SBA-15 (n, m) was produced, where n represents the reaction time (h) and m represents the reaction temperature (K).

The titania loading on mesoporous aluminosilicate Al-SBA-15 and silicate SBA-15 was measured using the ammonium sulfate–sulfuric acid digestion method [24].

2.4. Characterization

The crystalline phase of samples were analyzed by powder X-ray diffraction on a Bruker AXS D8 Advance X-ray diffractometer with a Cu Kα radiation source, at a speed of 2°/min within the range from 10° to 80° in 2θ. Nitrogen adsorption and desorption isotherms at 77 K were performed using an ASAP 2010 volumetric adsorption analyzer after samples had been degassed at 473 K for 2 h. The pore size distribution data were calculated by the BJH model from N_2 desorption isotherms. The solid-state NMR experiment was carried out at $B_0=9.4$ T on a Bruker AVANCE III 400 WB spectrometer. The corresponding resonance frequency of ^{27}Al was 104.3 MHz. The sample morphology was examined by means of transmission electron microscopy (TEM, JEM-2100F) at an accelerating voltage of 200 kV. The UV–vis absorption spectra of the products were carried out on a Purkinje General T6 spectrophotometer (China). The UV–vis diffuse reflectance spectra were recorded on Hitachi U4100 UV–vis spectrophotometer using barium sulfate as standard.

2.5. Photocatalytic decolorization test

MB powder was dissolved in distilled water to make a stock solution of 20 mg/L. The pH value of MB solution was unregulated unless otherwise stated. Photocatalytic activity of samples was evaluated by batch experiments, using a LIMX-VII apparatus manufactured by Bylabo Precision Instrument Co. Ltd. (Xi'an, China). Under vigorously stirring, the mixture of 0.015 g catalyst and 30 mL MB solution was set in the dark for 30 min to guarantee the adsorption–desorption equilibrium between MB solution and photocatalyst before exposing to 500 W high-pressure mercury lamp with a wavelength of 365 nm, at an intensity of 156 μW/cm^2. The photocatalytic decolorization efficiency was checked through measurements of absorbance band of MB at 664 nm after a fixed irradiation time. The absorbance measurement of reaction solutions was performed after separating catalyst from reaction suspensions by centrifugation for 15 min (12,000 r min^{-1}).

3. Results and discussion

3.1. ^{27}Al MAS NMR

Fig. 2 depicts the ^{27}Al MAS NMR spectrum of the Al-SBA-15 sample. It exhibits two obvious signals at ca. $\delta=0$ ppm from octahedral AlO_6 groups corresponding to extra-framework aluminum species and ca. $\delta=52.9$ ppm from tetrahedral aluminum species of AlO_4 units [25], respectively. The presence of last signal demonstrates that most aluminum ions have been effectively incorporated into the virgin SBA-15 framework, as we expected.

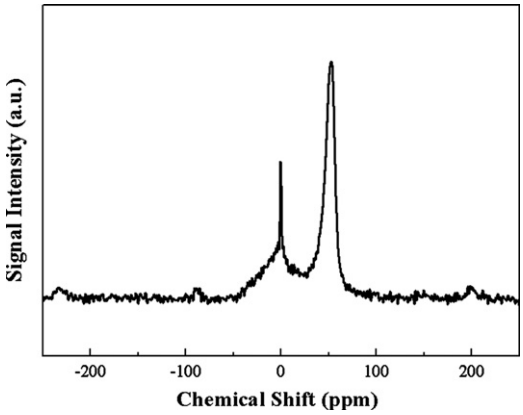

Fig. 2. ^{27}Al MAS NMR spectrum of the Al-SBA-15 sample.

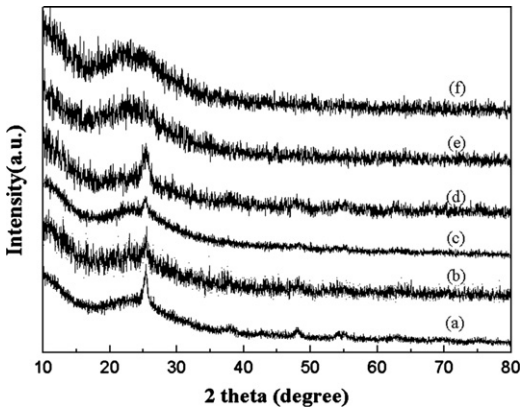

Fig. 3. XRD patterns of (a) 2 h, 313 K, (b) 4 h, 313 K, (c) 8 h, 313 K, (d) 4 h, 323 K, (e) 4 h, 333 K, and (f) 4 h, 343 K.

3.2. XRD patterns

Fig. 3 represents the wide angle X-ray powder diffraction patterns of synthesized TiO_2/Al-SBA-15 samples. Pure Al-SBA-15 exhibits a single broad peak, characteristic of amorphous silica [26]. Samples TiO_2–Al-SBA-15 (2, 313), TiO_2–Al-SBA-15 (4, 313), TiO_2–Al-SBA-15 (8, 313), and TiO_2–Al-SBA-15 (4, 323) shows evident peaks centered at 25.3° (101), 37.8° (004), assigning to characteristic diffraction of anatase TiO_2 phase [27], which are not observed in other samples. In addition, the intensity of anatase peak at 25.3° gradually decreases with increase of the reaction time and temperature, which tallies well with the variation of titania loading in Table 1, indicating that short reaction time and low temperature are beneficial to enhance the titania content over Al-SBA-15. The titania crystalline size is calculated to be nearly 10 nm, a little larger than the average pore size of about 6 nm in Table 1. As a result, we

Table 1
The specific surface areas (A_{BET}), pore volume (V_{BJH}) and pore size (D_{BJH}) of samples SBA-15, Al-SBA-15, and TiO_2/Al-SBA-15.

Samples	A_{BET} (m^2/g)	V_{BJH} (mL/g)	D_{BJH} (nm)	Titania content (%)	E_g (eV)
Al-SBA-15	752	1.06	6.85	0	–
TiO_2/SBA-15(4, 323)	389	1.08	8.03	4.1	3.36
TiO_2/Al-SBA-15(2, 313)	463	0.64	6.52	18.1	3.43
TiO_2/Al-SBA-15(4, 313)	471	0.71	6.13	17.8	3.28
TiO_2/Al-SBA-15(8, 313)	570	0.85	6.54	13.3	3.35
TiO_2/Al-SBA-15(4, 323)	517	0.66	5.46	21.7	3.13
TiO_2/Al-SBA-15(4, 333)	529	0.73	6.03	6.6	3.25
TiO_2/Al-SBA-15(4, 343)	632	0.88	6.08	3.3	3.01

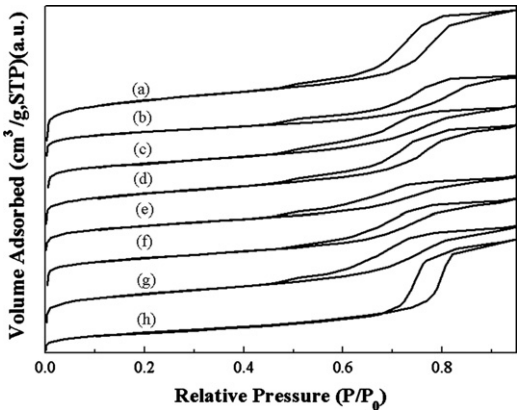

Fig. 4. N_2 adsorption/desorption isotherms of Al-SBA-15 and various TiO_2/Al-SBA-15 catalysts synthesized at different times and temperatures by supercritical CO_2: (a) Al-SBA-15, (b) 2 h, 313 K, (c) 4 h, 313 K, (d) 8 h, 313 K, (e) 4 h, 323 K, (f) 4 h, 333 K, and (g) 4 h, 343 K.

concluded that anatase phase with big crystallite size was formed on the external surface and small crystallite sized or amorphous anatase phase was distributed inside the channels, leading to the shrinkage of pore size as in Table 1.

3.3. Nitrogen adsorption

Fig. 4 displays the N_2 adsorption–desorption isotherms of Al-SBA-15, TiO_2/SBA-15 and TiO_2/Al-SBA-15 samples. It is clearly observed that all TiO_2/Al-SBA-15 examples represent the type IV isotherm according to IUPAC classification and type H1 hysteresis loop at relative pressure P/P^0 ranging from 0.5 to 0.9, indicative of uniformly mesoporous samples at the capillary condensation step [28]. While sample TiO_2/SBA-15 shows a type H1 hysteresis loop at relative pressure P/P^0 ranging from 0.6 to 0.9. The hysteresis is as a result of the existence of the ink-bottle pores [29]. Fig. 5 shows the pore size distribution of Al-SBA-15 and TiO_2/Al-SBA-15 samples. The pore width of TiO_2/Al-SBA-15 samples was slightly shrank or close to original Al-SBA-15, informing small crystalline or amorphous TiO_2 might incorporate into the mesopores, in accordance with the XRD results.

Table 1 shows the textural properties of sample Al-SBA-15, TiO_2/SBA-15, and TiO_2/Al-SBA-15. A_{BET} value 389 m^2/g of TiO_2/SBA-15 is smaller than those of TiO_2/Al-SBA-15 samples, as a result of the substitution of Si^{4+} species with Al^{3+} ions, which is in line with the Ref. [14]. The specific surface area of TiO_2/Al-SBA-15 gradually decreases compared to that of Al-SBA-15, indicating the planting small crystallite anatase or amorphous semiconductor within the ordered channels of the support [30]. A slight increase of the pore volume with the increase of the synthesized time and temperature, which is well consistent with the relatively low content of titania loading over the mesoporous samples. However, the variation of pore diameter from different samples is somewhat out of accord with the titania content, possibly attributing to the coexistence of big crystallite sized anatase outside the channels and small crystallite sized or amorphous anatase inside the channels, as stated above. From the Table 1, the content of titania loading on Al-SBA-15 decreased with the extension of reaction time, which might be owning to the fact that prolonging the reaction time was beneficial to export instead of import of titanium precursor by Sc-CO_2. Meanwhile, temperature was another effect on the content of TiO_2 loading. In our experimental, raising temperature upto 323 K could enhance the TiO_2 content, but further raising temperature could contrarily reduce the TiO_2 content, possibly owning to the comprehensive effect of low dissolving capability and high mass transfer of Sc-CO_2 under a high temperature.

3.4. UV–vis diffuse reflectance spectra

The UV–vis diffuse reflectance spectra of various different samples TiO_2/SBA-15 and TiO_2/Al-SBA-15 are shown in Fig. 6. Some samples containing small crystallite sized or amorphous anatase titania inside the channels like TiO_2/SBA-15(4, 323) and TiO_2/Al-SBA-15(2, 313) exhibit an absorption edge of less than 375 nm, indicating blue shifts from the absorption edge of bulk anatase titania by well known quantum size effect for semiconductors along with the decrease of particles size [31,32]. Other samples show an absorption edge of over 375 nm, attributing to the existence of big crystallite sized anatase outside the channels in these samples. These are in accordance with the results of XRD patterns and TEM measurements in the following section. The corresponding band gap

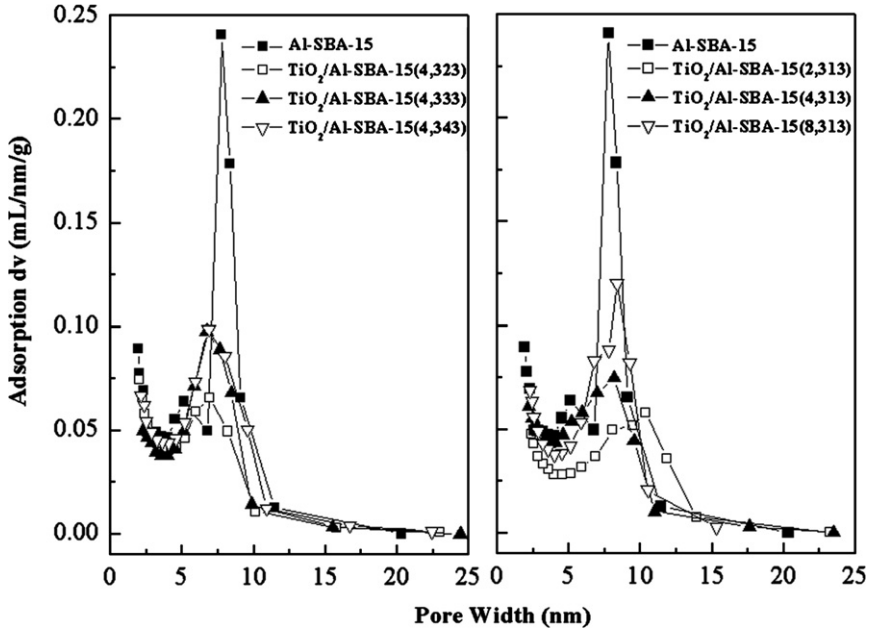

Fig. 5. Pore size distribution of Al-SBA-15 and TiO_2/Al-SBA-15: (a) synthesized at different temperature, and (b) synthesized at different time.

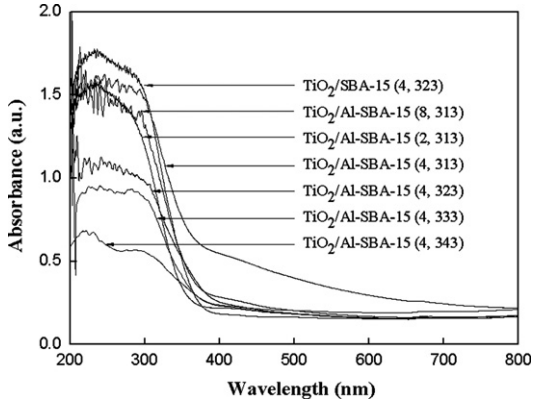

Fig. 6. The UV–vis diffuse reflectance spectra of various samples TiO_2/SBA-15 and TiO_2/Al-SBA-15.

energies were calculated according to the relation $E_g = 1240/\lambda$ onset and were listed in the Table 1.

3.5. TEM

Fig. 7 shows the microstructures of sample TiO_2/Al-SBA-15 synthesized at the temperature of 323 K and the time of 4 h. It is apparently discerned the presence of small titania nanoparticles inside the stripe patterns of Al-SBA-15 structure as black spots and large titania nanoparticles on the external surface of Al-SBA-15 as bulk forms. The micrographs of sample TiO_2/Al-SBA-15 show well-ordered hexagonal arrays of mesopores, indicative of a 2D hexagonal mesostructure without destruction even after titania loading. The pore diameter estimated from the micrograph is around 6 nm, which is in a good accordance with the N_2 adsorption measurement.

3.6. Photocatalytic decolorization of MB

Fig. 8 shows the photocatalytic decolorization capability of synthesized samples over cationic dye MB. It is obvious that all samples display satisfactory removal efficiency. After 80 min, all samples could accomplish the complete decolorization of MB under the same experimental condition. The samples TiO_2/Al-SBA-15(4, 323) with 21.7% titania content and TiO_2/Al-SBA-15(8, 313) with 3.3% titania content show the highest and lowest removal efficiency upon MB, respectively. As a result, the photodegradable capability of samples was partially associated with the TiO_2 content on Al-SBA-15, that is to say, with the variation of number of active cites.

Fig. 9 shows the comparative study of the photocatalytic decolorization capability of TiO_2/Al-SBA-15(4, 323), TiO_2/SBA-15(4, 323), and commercial TiO_2 on MB. It is apparent that both adsorption and degradable capability of TiO_2/Al-SBA-15(4, 323) are much higher than TiO_2/SBA-15(4, 323) and commercial TiO_2 as well. It can be explained by the following reasons. Much large specific surface area of TiO_2/Al-SBA-15 samples show strong adsorption capability not only on the dye molecules, but also on the significant amounts of water and hydroxyl groups around the active sites, thus enhance degradable efficiency [33]. We have tried a comparative study of MB adsorption on both Al-SBA-15 and SBA-15 and found that much higher adsorption capability on MB was observed using Al-SBA-15 as a sorbent. In this sense, even lower titania content on Al-SBA-15 still shows higher photocatalytic degradability comparing to sample TiO_2/SBA-15. Meanwhile, mesopores in the framework of TiO_2/Al-SBA-15 facilitates the import of dye molecules and export of degraded species and therefore facilitate the

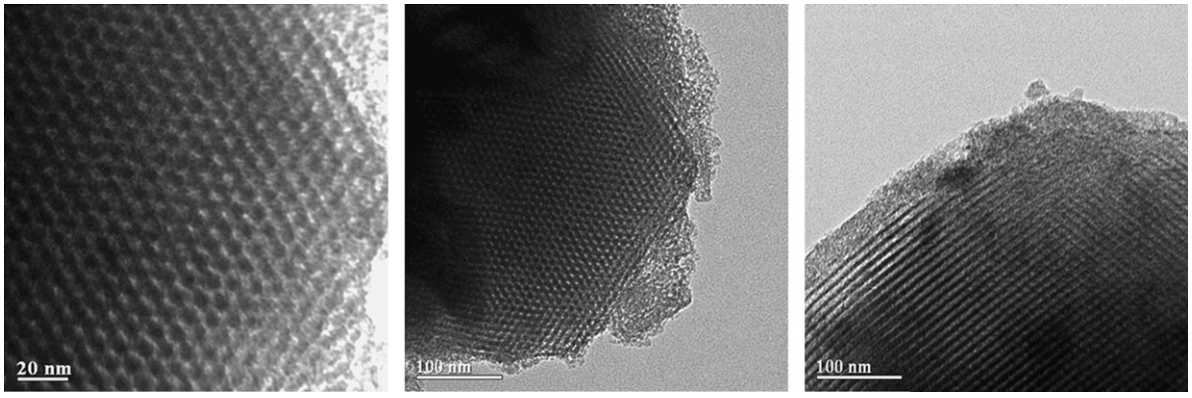

Fig. 7. TEM images of TiO_2/Al-SBA-15(4, 323).

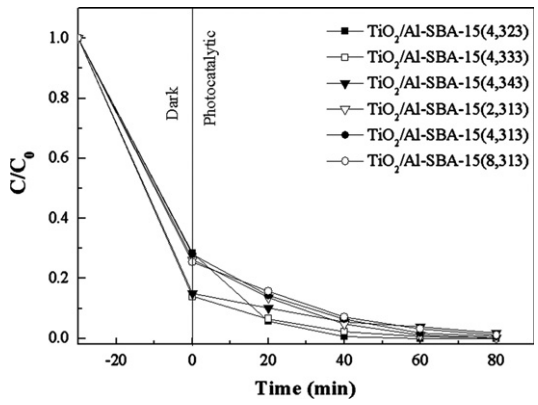

Fig. 8. The photocatalytic capability of samples TiO_2/Al-SBA-15 on the decomposition of MB.

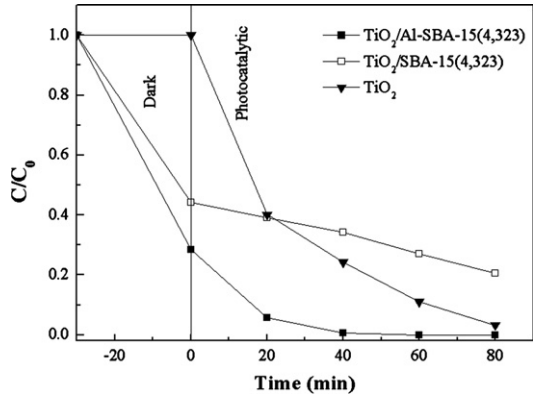

Fig. 9. The photocatalytic capability of samples TiO_2/Al-SBA-15, TiO_2/SBA-15, and commercial TiO_2 on the decomposition of MB.

photodecolorization process [22]. In addition, titania nanoparticles dispersed over the mesoporous materials own a high specific surface area and are thus beneficial to the photodecolorization as well [34]. As a result, presence of regular mesopores, confined titania nanoparticles, and large specific surface area together contributed to the enhanced photocatalytic degradability of TiO_2/Al-SBA-15 in comparison with TiO_2/SBA-15 and commercial TiO_2. Coupling with the simple preparation using a green technique and excellent photocatalytic degradability, TiO_2/Al-SBA-15 may have potential employments in the field of environmental protection and remediation in the future.

4. Conclusions

The preparation of titania nanoparticles on mesoporous aluminosilicate Al-SBA-15 in Sc-CO_2 was first reported in this present study and the resultant samples were characterized by a combination of various techniques. The aluminum species incorporated samples maintained a structure similar to that of the original SBA-15. The content of titania loading on Al-SBA-15 changed along with the reaction temperature and time in Sc-CO_2. From the analysis, large crystalline sized titania nanoparticles were formed on the external surface and small crystalline sized titania nanoparticles or amorphous titania were incorporated into the mesopores. The as-prepared samples were evaluated with regard to photocatalytic decolorization of MB in aqueous solutions. All TiO_2/Al-SBA-15 samples showed satisfactory decolorization efficiency, which was much better than TiO_2/SBA-15 and commercial TiO_2 under the same condition. The phenomenon may possibly own to the presence of regular mesopores, confined titania nanoparticles, and large specific surface area.

Acknowledgments

We are grateful to the National Natural Science Foundation of China (Grant no's 21207089, 51073175, 41076040, and 20807036), the Innovation Program of Shanghai Municipal Education Commission (Grant number 11YZ113), the Special Research Fund in Shanghai Colleges and Universities to Select and Train Outstanding Young Teachers (Grant number slg10014), and the project-sponsored by SRF for ROCS, SEM for financial support.

References

[1] M.R. Hoffmann, S.T. Martin, W.Y. Choi, D.W. Bahnemann, Environmental applications of semiconductor photocatalysis, Chemical Reviews 95 (1995) 69–96.

[2] T.L. Thompson, J.T. Tates Jr., Surface science studies of the photoactivation of TiO_2–new photochemical processes, Chemical Reviews 106 (2006) 4428–4453.
[3] O. Legrini, E. Oliveros, A.M. Braun, Photochemical processes for water treatment, Chemical Reviews 93 (1993) 671–698.
[4] M.N. Chong, B. Jin, C.W.K. Chow, C. Saint, Recent developments in photocatalytic water treatment technology: a review, Water Research 44 (2010) 2997–3027.
[5] F. Han, V.S.R. Kambala, M. Srinivasan, D. Rajarathnam, R. Naidu, Tailored titanium dioxide photocatalysts for the degradation of organic dyes in wastewater treatment: a review, Applied Catalysis A 359 (2009) 25–40.
[6] G. Jiang, Z. Lin, C. Chen, L. Zhu, Q. Chang, N. Wang, W. Wei, H. Tang, TiO_2 nanoparticles assembled on graphene oxide nanosheets with high photocatalytic activity for removal of pollutants, Carbon 49 (2011) 2693–2701.
[7] D. Zhao, Q. Huo, J. Feng, B.F. Chmelka, G.D. Stucky, Nonionic triblock and star diblock copolymer and oligomeric surfactant syntheses of highly ordered, hydrothermally stable, mesoporous silica structures, Journal of the American Chemical Society 120 (1998) 6024–6036.
[8] D. Zhao, J. Feng, Q. Huo, N. Melosh, G.H. Fredrickson, B.F. Chmelka, G.D. Stucky, Triblock copolymer syntheses of mesoporous silica with periodic 50–300 angstrom pores, Science 279 (1998) 548–552.
[9] M.H. Huang, A. Choudrey, P. Yang, Ag nanowire formation within mesoporous silica, Chemical Communications 12 (2000) 1063–1064.
[10] X. Yang, W. Dai, R. Gao, K. Fan, Characterization and catalytic behavior of highly active tungsten-doped SBA-15 catalyst in the synthesis of glutaraldehyde using an anhydrous approach, Journal of Catalysis 249 (2007) 278–288.
[11] P. Shukla, S. Wang, H. Sun, H.-M. Ang, M. Tadé, Adsorption and heterogeneous advanced oxidation of phenolic contaminants using Fe loaded mesoporous SBA-15 and H_2O_2, Chemical Engineering Journal 164 (2010) 255–260.
[12] Z. Luan, M. Hartmann, D. Zhao, W. Zhou, L. Kevan, Alumination and ion exchange of mesoporous SBA-15 molecular sieves, Chemistry of Materials 11 (6) (1999) 1621–1627.
[13] T. Jiang, H. Tao, J. Ren, X. Liu, Y. Wang, G. Lu, Fluoride ions assistant synthesis of extremely hydrothermal stable Al-SBA-15 with controllable Al content, Microporous and Mesoporous Materials 142 (2011) 341–346.
[14] G.M. Kumaran, S. Garg, K. Soni, M. Kumar, J.K. Gupta, L.D. Sharma, K.S.R. Rao, G.M. Dhar, Synthesis and characterization of acidic properties of Al-SBA-15 materials with varying Si/Al ratios, Microporous and Mesoporous Materials 114 (2008) 103–109.
[15] P. Bhangea, D.S. Bhange, S. Pradhan, V. Ramaswamy, Direct synthesis of well-ordered mesoporous Al-SBA-15 and its correlation with the catalytic activity, Applied Catalysis A: General 400 (2011) 176–184.
[16] A. Olivas, T.A. Zepeda, Impact of Al and Ti ions on the dispersion and performance of supported NiMo(W)/SBA-15 catalysts in the HDS and HYD reactions, Catalysis Today 143 (2009) 120–125.
[17] Y. Li, D. Pan, C. Yu, Y. Fan, X. Bao, Synthesis and hydrodesulfurization properties of NiW catalyst supported on high-aluminum-content, highly ordered, and hydrothermally stable Al-SBA-15, Journal of Catalysis 286 (2012) 124–136.
[18] E. Reverchon, R. Adami, Nanomaterials and supercritical fluids, Journal of Supercritical Fluids 37 (2006) 1–22.
[19] F. Cansell, C. Aymonier, Design of functional nanostructured materials using supercritical fluids, Journal of Supercritical Fluids 47 (2009) 508–516.
[20] P. López-Aranguren, J. Saurina, L.F. Vega, C. Domingo, Sorption of tryalkoxysilane in low-cost porous silicates using a supercritical CO_2 method, Microporous and Mesoporous Materials 148 (2012) 15–24.
[21] J. Feng, G. An, B. Chen, Y. Li, K. Ding, Y. Xie, Z. Liu, Post-synthesis of Ti-SBA-15 in supercritical CO_2–ethanol solution, Clean—Soil, Air, Water 37 (2009) 527–533.
[22] D. Sun, Z. Liu, J. He, B. Han, J. Zhang, Y. Huang, Surface sol–gel modification of mesoporous silica molecular sieve SBA-15 with TiO_2 in supercritical CO_2, Microporous and Mesoporous Materials 80 (2005) 165–171.
[23] Y. Yue, A. Gédéon, J.L. Bonardet, J.B. D'Espinose, J. Fraissard, N. Melosh, Direct synthesis of AlSBA mesoporous molecular sieves: characterization and catalytic activities, Chemical Communications 19 (1999) 1967–1968.
[24] J.M. Coronado, M.E. Zorn, I. Tejedor-Tejedor, M.A. Anderson, Photocatalytic oxidation of ketones in the gas phase over TiO_2 thin films: a kinetic study on the influence of water vapor, Applied Catalysis B: Environmental 43 (2003) 329–344.
[25] W. Hu, Q. Luo, Y. Su, L. Chen, Y. Yue, C. Ye, F. Deng, Acid sites in mesoporous Al-SBA-15 material as revealed by solid-state NMR spectroscopy, Microporous and Mesoporous Materials 92 (2006) 22–30.
[26] F. Chiker, J.P. Nogier, F. Launay, J. Bonardet, New Ti-SBA mesoporous solids functionnalized under gas phase conditions: characterisation and application to selective oxidation of alkenes, Applied Catalysis A: General 243 (2003) 309–321.
[27] H.D. Nam, B.H. Lee, S.J. Kim, C.H. Jung, J.H. Lee, S. Park, Preparation of ultrafine crystalline TiO_2 powders from aqueous $TiCl_4$ solution by precipitation, Japanese Journal of Applied Physics 37 (1998) 4603–4608.
[28] S.J. Gregg, K.S.W. Sing, in: Adsorption Surface Area and Porosity, Academic Press, London, New York, 1982.
[29] T. Lopez, F. Rojas, R. Alexander-Katz, F. Galindo, A. Balankin, A. Buljan, Porosity, structural and fractal study of sol–gel TiO_2–CeO_2 mixed oxides, Journal of Solid State Chemistry 177 (2004) 1873–1885.
[30] W.Y. Jung, S.H. Baek, J.S. Yang, K.T. Lim, M.S. Lee, G.D. Lee, S.S. Park, S.S. Hong, Synthesis of Ti-containing SBA-15 materials and studies on their photocatalytic decomposition of orange II, Catalysis Today 131 (2008) 437–443.
[31] A. Tuel, L.G. Hubert-Pfalzgraf, Nanometric monodispersed titanium oxide particles on mesoporous silica: synthesis, characterization, and catalytic activity in oxidation reactions in the liquid phase, Journal of Catalysis 217 (2003) 343–353.
[32] W. Wang, M. Song, Photocatalytic activity of titania-containing mesoporous SBA-15 silica, Microporous and Mesoporous Materials 96 (2006) 255–261.
[33] J. Yang, J. Zhang, L. Zhu, S. Chen, Y. Zhang, Y. Yu Tang, Y. Zhu, Y. Li, Synthesis of nano titania particles embedded in mesoporous SBA-15: characterization and photocatalytic activity, Journal of Hazardous Materials 137 (2006) 952–958.
[34] K. Nakat, A. Fujishima, TiO_2 photocatalysis: design and applications, Journal of Photochemistry and Photobiology C 13 (2012) 169–189.